

# Lyapunov spectrum scaling for many-body dynamics close to integrability

Merab Malishava<sup>1,2\*</sup> and Sergej Flach<sup>1,2†</sup>

<sup>1</sup>Center for Theoretical Physics of Complex Systems, Institute for Basic Science(IBS), Daejeon, Korea, 34126

<sup>2</sup>Basic Science Program, Korea University of Science and Technology(UST), Daejeon, Korea, 34113

(Dated: June 4, 2025)

We use unitary map evolution to address the thermalization of many-body dynamical systems close to an integrable limit. Integrable limits are classified as either long-range or short-range, depending on the connectivity between actions. The connectivity type is imposed by the nonintegrable perturbation. We compute the Lyapunov spectra and analyze their scaling properties. Long-range limits result in a single parameter scaling of the Lyapunov spectrum, with the largest Lyapunov exponent being the only control parameter. Short-range networks have an additional second scaling parameter which describes the exponential suppression of all relative to the largest Lyapunov exponent.

Thermalization is a universal property of the long-time dynamics of generic nonintegrable many-body systems. Thermal equilibrium is characterized by stationary distributions and assumes ergodicity and mixing in the phase space [1]. The thermalization dynamics will in general slow down close to integrability, and may even cease to be observed [2–8], which was also noted in earlier studies of dynamical systems [9–12]. The theory of weak nonintegrable perturbations for finite Hamiltonian systems was pioneered by Kolmogorov in 1954 [13] and later by Arnold [14] and Moser [15]. The corresponding KAM theory demonstrates the violation of the ergodic hypothesis for sufficiently weak perturbations due to the emergence of a mixed phase space with a finite fraction of points belonging to regular trajectories on tori. At a critical strength of the nonintegrable perturbation, all tori disappear, and the dynamics become fully chaotic allowing for thermalization. But what exactly is meant by “sufficiently weak” and “critical strength”? As it turns out the magnitude of the critical perturbation  $\tilde{H}$  decays rapidly with the growth of the number of degrees of freedom. Namely,  $|\tilde{H}| \leq aN^{-b}$  with  $b = 160$  has been shown as an upper bound for applicability of KAM theory in lattice systems with short-range interactions (for example an array of Josephson junctions) [16]. This result suggests that it is practically impossible to witness quasiperiodic motion suggested by KAM in macroscopically large systems close to integrability. What is then the expected behavior of systems with a large number of degrees of freedom in proximity to an integrable limit? How does one characterize it? Does it have universality classes? Is there a KAM-like regime for macroscopic models? If not, what lies beyond the KAM horizon spanned by finite systems?

An integrable system is characterized by a corresponding set of conserved actions. It can be viewed as a graph of disconnected nodes, with each node corresponding to

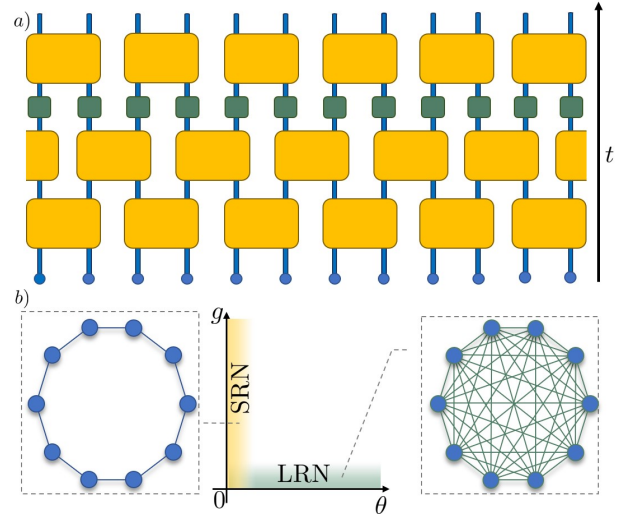


FIG. 1. a) A schematic representation of the unitary circuits evolution. Large yellow blocks indicate  $\hat{C}$  pair operators parametrized by the angle  $\theta$ . Small green blocks indicate local nonlinearity generating operators  $\hat{G}$  parametrized by the nonlinearity strength coefficient  $g$ . The black arrow on the right indicates the time flow. b) Control parameter space  $\{\theta, g\}$  with the highlighted area corresponding to the induced networks. Integrable limits are reached for  $g = 0$  (linear evolution of extended normal modes) or  $\theta = 0$  (decoupled nonlinear oscillators). Small nonzero  $g$  values induce LRNs, small nonzero  $\theta$  values induce SRNs. The network images indicate actions (filled circles) and couplings induced by the nonintegrable perturbation (straight lines). Left image - SRN, right image - LRN.

an action. Adding a nonintegrable perturbation amounts to inducing couplings between actions which are manifested as the edges of the graph. The coupling range then becomes a major classifier of the perturbation [17]. Hereinafter we will call a network whose number of couplings scales with the system size – a long-range network (LRN). Otherwise, the network will be called short-range (SRN). Examples of SRNs include anharmonic oscillator chains in the limit of weak coupling [17], Josephson junction chains in the limit of weak coupling or large energy

\* Corresponding author:  
merabmalishava@gmail.com

† Corresponding author:  
sergejflach@googlemail.com

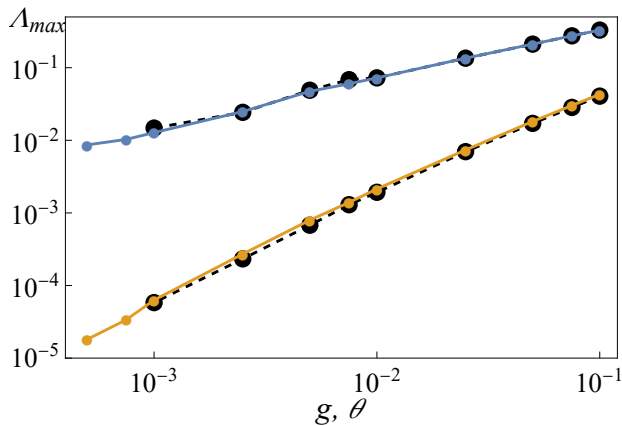


FIG. 2. The largest Lyapunov exponents  $\Lambda_{\max}$  in SRN (blue small circles, top) and LRN (orange small circles, bottom) regime versus the corresponding deviation from integrable limit  $g, \theta$ . Solid lines connect the data points and guide the eye. For the SRN case, the parameter nonlinearity is fixed  $g = 1.0$ , while for the LRN case the angle  $\theta$  is fixed at  $0.33\pi$ . For both cases system size  $N = 200$ . The large black circles connect by dashed lines correspond to data for system size  $N = 100$ .

density [18], etc. The local nature of the interaction ensures the short range of the network. On the other hand, extended systems [19] serve as a hallmark for studies of quantum chaos in all-to-all interaction models [20–22], which are typical examples of LRNs, along with translationally invariant lattice systems in the limit of weak nonlinear perturbations [17, 18]. Typically, physical models close to integrability belong to either of the two classes.

The network range plays a defining role in the thermalization dynamics of the system. Previous studies focused on the evolution of finite time averages of observables [17, 18]. By choosing the actions of the integrable limit as observables, one can study the slowing down of the evolution upon approaching the integrable limit. One major outcome was that for LRNs the slowing down is correlated to the changes of the largest Lyapunov exponent, while for SRNs an additional resonance diffusion resulted in a decoupling of the slowing down from the much shorter inverse largest Lyapunov exponent [23]. As the precise choice of the observables remains ambiguous (one could use any combinations or functions of the above actions) we lack clear universal diagnostic tools to distinguish SRNs from LRNs. Is it possible to identify all relevant time scales of the underlying dynamics of a generic weakly nonintegrable macroscopic system and thus assert the nature of a network of observables? In this Letter, we obtain a positive answer by analyzing the scaling properties of the entire Lyapunov spectrum and in particular of the Kolmogorov-Sinai entropy which depend on the chosen network type. We use highly efficient unitary maps to access the very vicinity of integrable limits of large dynamical systems.

*Model* – We perform our investigations using unitary

map evolution. The key feature of unitary maps is a discrete time-space evolution protocol. This results in an extremely efficient numerical implementation [24]. These properties make unitary maps stand out as a tool for simulating such phenomena as Anderson localization during wave propagation [25, 26], soliton dynamics [27] and others. We will enrich the above list by adding the efficient computation of the entire Lyapunov spectrum through the evolution of tangent vectors using Unitary Circuits (UC).

The system consists of a 1D array of size  $N$  with one component wave function  $|\Psi\rangle = \sum_n \psi_n |n\rangle$  per site. The phase space of the dynamical system is equivalent to the Hilbert space which embeds  $|\Psi\rangle$ . The dynamics are induced by subsequent applications of the evolution operator:

$$\hat{U} = \sum_{n \in \mathbb{Z}} \hat{G}_n \sum_{n \in 2\mathbb{Z}+1} \hat{C}_{n,n+1} \sum_{n \in 2\mathbb{Z}} \hat{C}_{n,n+1}. \quad (1)$$

Operators  $\hat{C}_{n,n+1}$  represent quantum gates given by a  $2 \times 2$  orthogonal matrix parametrized by the rotation angle  $\theta$ :

$$\hat{C}_{n,n+1} = \begin{pmatrix} \cos \theta & \sin \theta \\ -\sin \theta & \cos \theta \end{pmatrix}, \quad (2)$$

and operators  $G_n$  induce nonlinearity:

$$\hat{G}_n = e^{ig|\psi_n|^2} |n\rangle \langle n|. \quad (3)$$

The unitary circuit dynamics is schematically represented in Fig. 1.

*SRN integrable limit* – We consider the limiting case  $\theta = 0$  with a fixed nonzero value of nonlinearity strength  $g$ . In this setup the operators  $\hat{C}_{n,n+1}$  become unity matrices, thus decoupling the sites. The unitary evolution operator applies a nonlinear norm dependent phase shift at each site:

$$\hat{U}_{\text{int}}^{\text{SRN}} = \sum_{n \in \mathbb{Z}} e^{ig|\psi_n|^2} |n\rangle \langle n|. \quad (4)$$

The system turns integrable with the norm at each site  $|\psi_n|$  being a constant of motion. By introducing a weak deviation from the limit  $0 < \theta \ll 1$  one induces a network with nearest-neighbor interaction - an SRN (see Supplemental Material for more details [28]). We schematically represent the parameter space and corresponding network in Fig. 1(b).

*LRN integrable limit* – Vanishing nonlinearity strength  $g = 0$  results in a linear evolution with corresponding eigenvalue problem  $e^{i\omega} |\Psi(t)\rangle = \hat{U}_{\text{int}}^{\text{LRN}} |\Psi(t)\rangle$  (see details in Supplemental Material [28]). The evolution operator corresponding to this integrable limit is given by:

$$\hat{U}_{\text{int}}^{\text{LRN}} = \sum_k \hat{u}_k |\psi_k\rangle \langle \psi_k|, \quad (5)$$

where  $|\psi_k\rangle$  are the normal modes of the system and  $u_k$  is the evolution operator in reciprocal space corresponding to the wavenumber  $k$ . In this limit the absolute values

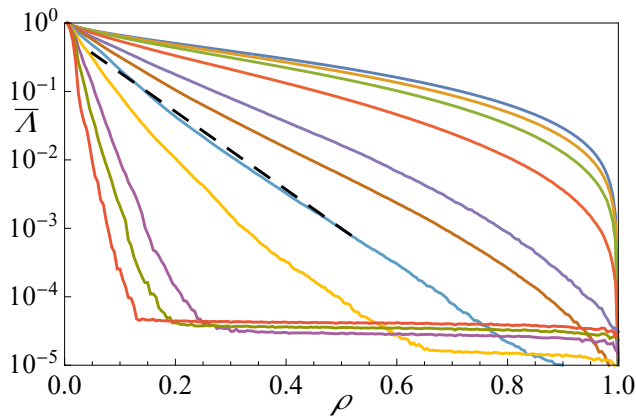


FIG. 3. Renormalized Lyapunov spectrum  $\{\bar{\Lambda}_i\}$  for SRN in proximity to the integrable limit. The nonlinearity strength is fixed at  $g = 1.0$ . Angle  $\theta$  varies from  $10^{-1}$  (blue, top) to  $5 \cdot 10^{-4}$  (red, bottom). The inset shows the coefficient  $1/\beta$  of the exponential decay (see also Fig. 4) of the curves as a function of  $\theta$ . System size  $N = 200$ .

of the normal mode amplitudes  $|c_k| = |\langle \psi_k | \Psi(t) \rangle|$  are the constants of motion. The deviation from this limit  $g \neq 0$  induces an all-to-all coupling among the normal modes of the system which respects translational invariance through selection rules [28]. This by definition constitutes an LRN. The green region in the control parameter space in Fig. 1(b) corresponds to that LRN with the schematic representation of the network sketched right to it.

*Lyapunov spectrum* – Chaotic dynamics diagnostics usually focuses on the maximal Lyapunov exponent, since it corresponds to the shortest characteristic time scale of chaotization. However, the resolution of the full spectrum allows to enter a whole new level of depth of insight into the underlying system dynamics. The Lyapunov spectrum was used as a diagnostic tool for energy localization [29] and has been analyzed using tools from random matrix theory [30]. Our motivation is to use the Lyapunov spectrum as a generic universal classifier of the thermalization dynamics of weakly nonintegrable macroscopic systems beyond the limits set by the KAM theory.

We compute the Lyapunov spectrum of Unitary Circuits in proximity to integrable limits in order to resolve the entire set of characteristic time scales. We follow the evolution of a set of orthogonal tangent vectors  $\{\vec{u}_i\}$  in the  $2N$  dimensional phase space and compute the increment  $\gamma_i(t) = |\vec{u}_i(t)|$ . Details on the approach can be found in Section ?? of the supplemental material [28]. For each vector we compute the transient value  $X_i(t) = 1/t \sum_{\tau} \log \gamma(\tau)$  which in the infinite time limit turns into the Lyapunov characteristic exponent (LCE)  $\Lambda_i = \lim_{t \rightarrow \infty} X_i(t)$ . The numerically computed LCEs are the values of  $X(t)$  extracted at the last step of the dynamics. The LCEs are ordered from largest to smallest

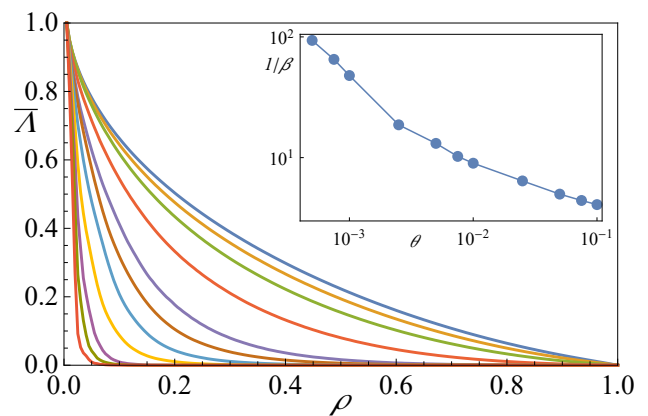


FIG. 4. Renormalized Lyapunov spectrum  $\{\bar{\Lambda}_i\}$  for SRN in log scale (corresponding to the parameters and data of Fig. 3). The dashed line is to guide the eye for the fit of exponential decay.

value upon incrementing the index  $i$ . Due to the symplectic nature of the map the spectrum is symmetric with LCEs coming in pairs  $\Lambda_i = -\Lambda_{2N-i+1}$ . Norm conservation ensures two vanishing LCEs  $\Lambda_N = \Lambda_{N+1} = 0$  [31]. According to the numerical setup, however, it is impossible to achieve exact  $\Lambda_i = 0$  values, with bounds on the smallest computed Lyapunov exponents  $\Lambda_{\min} \sim 1/t$ .

The evolution of the wave function  $|\Psi\rangle$  is obtained from subsequent applications of the operator  $\hat{U}$ . We use periodic boundary conditions  $\psi_{N+1} = \psi_1$ . The initial conditions for the amplitudes of the local components of the wave function are drawn from an exponential distribution  $p(x) = e^{-x}$ , while their phases were generated as uncorrelated and random numbers chosen uniformly from the interval  $[0, 2\pi]$ . The wave function is then uniformly rescaled such that the norm density  $\rho = \frac{1}{N} \sum |\psi_n|^2 = 1$ . The largest integration time varied between  $t_{\max} = 10^8$  and  $t_{\max} = 10^9$ . Unless stated otherwise the system size is set to  $N = 200$ .

First, we show the dependence of the largest Lyapunov exponent  $\Lambda_{max}$  on the distance  $g$  or  $\theta$  to the integrable limit in Fig. 2 for both networks. Both curves show a dependence which might resemble a power law  $\Lambda_{max} \sim g^\nu$  and  $\Lambda_{max} \sim \theta^\mu$  with  $\nu \approx 1/2$  and  $\mu \approx 3/2$ . Remarkably the SRN case shows a much slower diminishing of  $\Lambda_{max}$  upon approaching the integrable limit as compared to the LRN. This is similar to the study of a Hamiltonian system dynamics [17]. Our data in Fig.2 are obtained for two different system sizes  $N = 100, 200$  and show very good agreement, therefore we can exclude finite size corrections. We now proceed to the analysis of the entire Lyapunov spectrum. In Fig. 3 and Fig. 5 we show the renormalized Lyapunov spectrum  $\bar{\Lambda}_i = \Lambda_i/\Lambda_{max}$  for SRN and LRN respectively. The index of Lyapunov exponents is rescaled  $\rho = i/N$  so that all positive LCEs  $\bar{\Lambda}(\rho)$  correspond to  $\rho \in [0, 1]$ . We notice a dramatic qualitative difference between the two regimes. For the LRN case

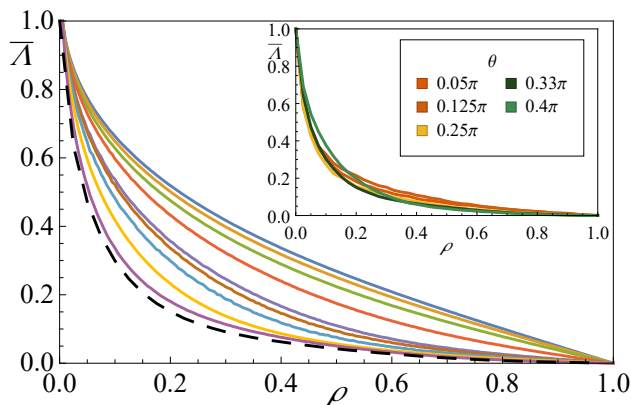


FIG. 5. Renormalized Lyapunov spectrum  $\{\bar{\Lambda}_i\}$  for LRN in proximity to the integrable limit. The angle  $\theta = 0.33\pi$  is fixed. The deviation from integrable limit  $g$  varies from  $10^{-1}$  (blue) to  $10^{-3}$  (purple). The dashed line is to show the asymptotic curve as  $g \rightarrow 0$ . In the inset we showcase the asymptotic curve as parameter  $\theta$  is varied. For all cases system size  $N = 200$ .

the renormalized Lyapunov spectrum  $\bar{\Lambda}(\rho)$  converges to a limiting smooth curve for  $g \rightarrow 0$ . For the SRN instead that curve vanishes in an exponential way. We will explain these observations in detail below.

For the SRN an increasing number of Lyapunov exponents seems to be vanishing upon approaching the integrable limit as seen in Fig.3. We replot the same spectrum in log scale in Fig. 4 and notice an exponential decay of the renormalized spectrum:

$$\Lambda_\rho^{\text{SRN}} = \Lambda_{\max} e^{-\rho/\beta}. \quad (6)$$

We fit the exponential decay and plot the exponent  $1/\beta$  versus  $\theta$  in the inset in Fig. 3. We observe that the exponent is rapidly diverging upon approaching the integrable limit such that  $\beta(\theta \rightarrow 0) \rightarrow 0$ . The entire Lyapunov spectrum of the SRN is therefore characterized by two scaling parameters - the largest Lyapunov exponent  $\Lambda_{\max}$  which is an inverse time scale, and the parameter  $\beta$  which is an inverse length scale. This result explains and agrees with previous studies on dynamical glass in Hamiltonian systems [17, 18] where the largest Lyapunov exponent stems from local resonances which rapidly increasing distance between them upon approaching the integrable limit. Our results show that the Lyapunov spectrum contains the quantitative scaling parameters of that dynamical glass theory.

In contrast, the LRN spectrum is characterized by single parameter scaling. The renormalized Lyapunov spectrum approaches a smooth limiting curve  $\bar{\Lambda}(\rho)$  as seen in Fig. 5. We compute the limiting curves by a linear fit of  $\bar{\Lambda}_\rho(g)$  at each value of  $\rho_j$ . Thus in the LRN regime, the

final form of the spectrum is given by:

$$\Lambda_\rho^{\text{LRN}} = \Lambda_{\max} f(\rho, \theta) \quad (7)$$

The limiting curves for different values of  $\theta$  are plotted in the inset of Fig.5 and show little if any variation. It appears that the limiting curve  $f(\rho)$  is universal for all LRN parameter choices.

To further characterize the chaotic dynamics and showcase the difference between SR and LR networks we compute the Kolmogorov-Sinai entropy  $K_{\text{KS}} = \int_0^1 \bar{\Lambda}_\rho d\rho$ . In the SRN case, from eq. (6) follows

$$K_{\text{KS}}^{\text{SRN}} = \Lambda_{\max} \beta (1 - e^{-1/\beta}). \quad (8)$$

Therefore the renormalized Kolmogorov-Sinai entropy  $k_{\text{KS}} = K_{\text{KS}}/\Lambda_{\max}$  will tend to zero in the integrable limit as which turns to  $k_{\text{KS}} \approx \beta$ .

In the LRN regime the integral over the asymptotic function  $f(\rho, \theta)$  (see eq. (7)) will lead to finite values of the renormalized KS entropy  $k_{\text{KS}} = \int_0^1 f(\rho) d\rho > 0$  at the very integrable limit.

*To conclude*, we identified the Lyapunov spectrum as a universal characteristic descriptor of the complex phase space dynamics of a macroscopic system in proximity to an integrable limit. The limit is characterized by a macroscopic number of conserved actions. We identify two classes of nonintegrable perturbation networks - short and long-range ones. Long-range networks are characterized by a single parameter scaling of the Lyapunov spectrum - knowing the largest Lyapunov exponent allows to reconstruct the entire spectrum. Consequently all Lyapunov exponents scale as the largest one upon approaching the integrable limit. Typical long-range networks are realized with translationally invariant lattice systems in the limit of weak nonlinearity. In that case, the actions correspond to normal modes extended over the entire real space. Nonintegrable perturbations will typically couple them all. On the other side, short-range networks are characterized by a two-parameter scaling. In addition to the largest Lyapunov exponent, a diverging length scale results in a suppression of the renormalized Lyapunov spectrum upon approaching the integrable limit. Typical short-range networks are realized with lattice systems and local (short-range) nonlinearities in the limit of weak coupling. Interestingly the short-range network case appears to include disordered systems as well. We, therefore, expect that disordered systems with weak short-range nonlinearities will correspond to the SRN universality class. Quantizing the classical dynamics could lead to many-body localization in the case of short-range networks, as opposed to long-range networks.

*Acknowledgments:* This work was supported by the Institute for Basic Science (Project number: IBS-R024-D1).

- 
- [1] K. Huang, *Statistical Mechanics*, 2nd ed. (John Wiley & Sons, 1987).
- [2] C. Gogolin, M. P. Müller, and J. Eisert, *Physical review letters* **106**, 040401 (2011).
- [3] M. Rigol, *Physical review letters* **103**, 100403 (2009).
- [4] D. K. Campbell, P. Rosenau, and G. M. Zaslavsky, *Chaos: An Interdisciplinary Journal of Nonlinear Science* **15**, 015101 (2005).
- [5] B. Gaveau and L. S. Schulman, *The European Physical Journal Special Topics* **224**, 891 (2015).
- [6] J.-P. Bouchaud, *Journal de Physique I* **2**, 1705 (1992).
- [7] G. Bel and E. Barkai, *EPL (Europhysics Letters)* **74**, 15 (2006).
- [8] G. Bel and E. Barkai, *Physical review letters* **94**, 240602 (2005).
- [9] J. Ford, *Physics Reports* **213**, 271 (1992).
- [10] N. J. Zabusky and G. S. Deem, *Journal of Computational Physics* **2**, 126 (1967).
- [11] M. Toda, *Journal of the Physical Society of Japan* **22**, 431 (1967), <https://doi.org/10.1143/JPSJ.22.431>.
- [12] M. Hénon and C. Heiles, *The Astronomical Journal* **69**, 73 (1964).
- [13] A. N. Kolmogorov, in *Dokl. Akad. Nauk SSSR*, Vol. 98 (1954) pp. 527–530.
- [14] V. I. Arnold, *Collected Works: Representations of Functions, Celestial Mechanics and KAM Theory, 1957–1965*, 267 (2009).
- [15] J. Moser, *Nachr. Akad. Wiss. Göttingen, II*, 1 (1962).
- [16] C. E. Wayne, *Communications in mathematical physics* **96**, 311 (1984).
- [17] C. Danieli, T. Mithun, Y. Kati, D. K. Campbell, and S. Flach, *Phys. Rev. E* **100**, 032217 (2019).
- [18] T. Mithun, C. Danieli, Y. Kati, and S. Flach, *Physical review letters* **122**, 054102 (2019).
- [19] S. Sachdev and J. Ye, *Physical review letters* **70**, 3339 (1993).
- [20] H. Guo, Y. Gu, and S. Sachdev, *Physical Review B* **100**, 045140 (2019).
- [21] B. Kobrin, Z. Yang, G. D. Kahanamoku-Meyer, C. T. Olund, J. E. Moore, D. Stanford, and N. Y. Yao, *Physical Review Letters* **126**, 030602 (2021).
- [22] Y. Gu, X.-L. Qi, and D. Stanford, *Journal of High Energy Physics* **2017**, 125 (2017).
- [23] T. Mithun, C. Danieli, M. V. Fistul, B. L. Altshuler, and S. Flach, *Phys. Rev. E* **104**, 014218 (2021).
- [24] I. Vakulchyk, M. V. Fistul, and S. Flach, *Physical review letters* **122**, 040501 (2019).
- [25] I. Vakulchyk, M. V. Fistul, P. Qin, and S. Flach, *Phys. Rev. B* **96**, 144204 (2017).
- [26] M. Malishava, I. Vakulchyk, M. Fistul, and S. Flach, *Physical Review B* **101**, 144201 (2020).
- [27] I. Vakulchyk, M. Fistul, Y. Zolotaryuk, and S. Flach, *Chaos: An Interdisciplinary Journal of Nonlinear Science* **28**, 123104 (2018).
- [28] See the Supplementary Material at the [URL].
- [29] S. Iubini and A. Politi, *Chaos, Solitons & Fractals* **147**, 110954 (2021).
- [30] M. Hanada, H. Shimada, and M. Tezuka, *Physical Review E* **97**, 022224 (2018).
- [31] C. Skokos, The lyapunov characteristic exponents and their computation, in *Dynamics of Small Solar System Bodies and Exoplanets*, edited by J. J. Souchay and R. Dvorak (Springer Berlin Heidelberg, Berlin, Heidelberg, 2010) pp. 63–135.